5.
A SINGLE SIDED DUAL ANTENNA STRUCTURE FOR UHF RFID TAGS

5.1. Introduction

In previous chapters three and four, it is observed that the single sided dual antenna structure mitigates the limitations of the single antenna structure utilized for RFID tags. Further, the study of the effect of mounting material such as metallic and non-metallic object is carried out to see the performance of tag antennas. The insignificant effect is observed on the input impedance of the tag antenna when it is mounted on plastic and paper surfaces whereas the input impedance significantly changes when the antenna is mounted on the metallic surface. However, the presented antenna is suitable for the mounting on paper, cardboard, and plastic materials but not suitable for metallic surfaces.

Since the dual antenna structures presented in chapter 3 and 4 are not compatible for the application with metallic surfaces as well as they do not have high differential RCS and gain; therefore, it is highly desirable to design a RFID tag antenna that can mitigate these limitations.

In the present chapter, a novel single sided dual antenna structure for UHF RFID tag is proposed for both metallic and non-metallic surfaces. The proposed tag consists of two independent antennas made up with two L-shaped strips, microstrip patch with a cross-shaped slot, ground plane, and a via. One antenna exclusively used for receiving and other for backscattering so that the requirements for the maximum and continuous power supply and maximum difference level of RCS in the backscattering mode can be achieved, simultaneously. Further, the RFID tag antennas are used with a variety of surfaces made of different materials. Therefore, an investigation is carried out to see the performance of proposed antenna in terms of RCS, gain, and read range when mounted on different materials like metal, plastic, wood, glass, etc.

5.2. Antenna Configuration

The configuration and fabricated prototype of the proposed antenna for RFID tag (Antenna-I) with dual antenna structure is shown in Figures 5.1(a) and 5.1(b), respectively. It is fabricated on the low-cost FR4 substrate with dielectric constant (ε_r) 4.4, loss tangent (tan δ=0.018) and thickness 1.6 mm. The proposed dual antenna consists of square patch loaded with a cross-shaped slot and two L-shaped open-ended microstripline of different lengths, connected to two terminals of tag chip and terminated by a shorting pin. The L-shaped lines are capacitively coupled to the patch as shown in Figure 5.1. The longer arm of the L-shaped microstripline is designed in such a way that the maximum power is coupled to the patch, and it acts as the receiving antenna whereas the small arm of L-shaped microstripline along with patch act as the backscattering antenna. The design concept of the proposed antenna in receiving mode is based on the paper reported in [Chen *et al*. (2012)], which is a conventional tag antenna.

Further, one of the major limitations of the microstrip antennas are the excitation of the surface waves which reduce the antenna efficiency, gain, and deteriorate the radiation patterns. The diffraction of surface waves from the edges of the antenna increases the back and side lobe radiations, which may reduce the signal to noise ratio in wireless communication systems [Yang and Samii (2009), Yang and Samii (2003)]. The surface wave propagation in microstrip antennas can be reduced significantly by using electromagnetic band gap (EBG) structures and can be used to enhance the gain and read range in the RFID system.

Therefore, to increase the gain of Antenna-I, mushroom-type EBG like structures are placed around the antenna which is referred as Antenna-II. Figure 5.2(a) and 5.2(b) show the geometry and fabricated prototype of proposed Antenna-II. The dimensions of the EBG unit cell are given in Figure 5.3. It is made of two C-shaped slots loaded square patch with a cylindrical via (1 mm diameter) which is shorted to the ground.

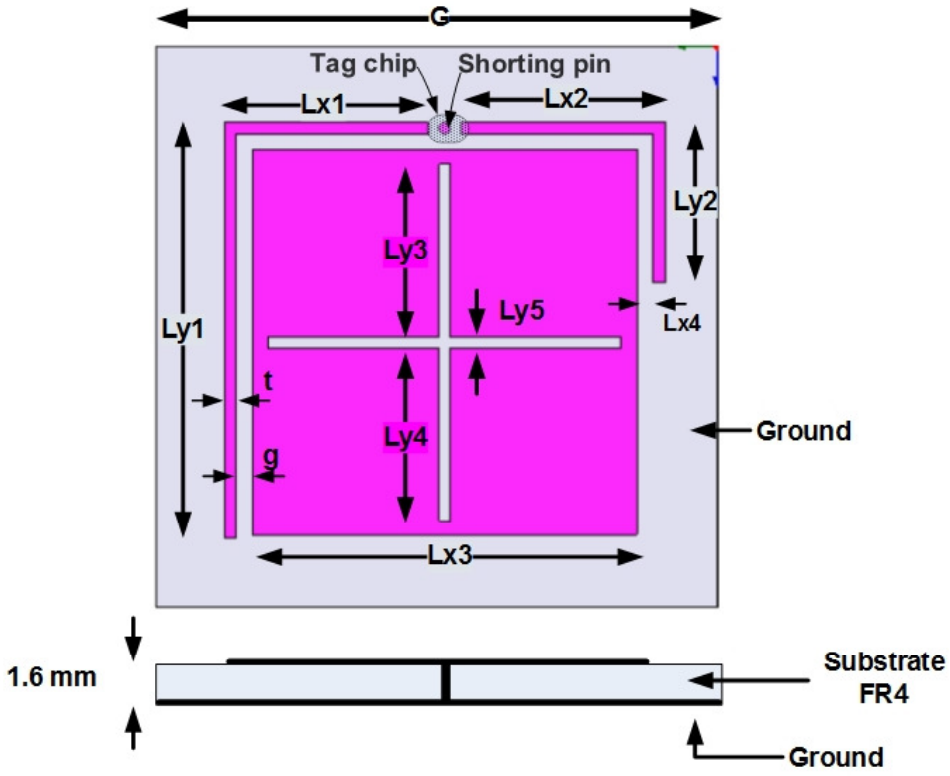

(a)

(b)

Figure 5.1: (a) Configuration and (b) fabricated prototype of the proposed Antenna-I

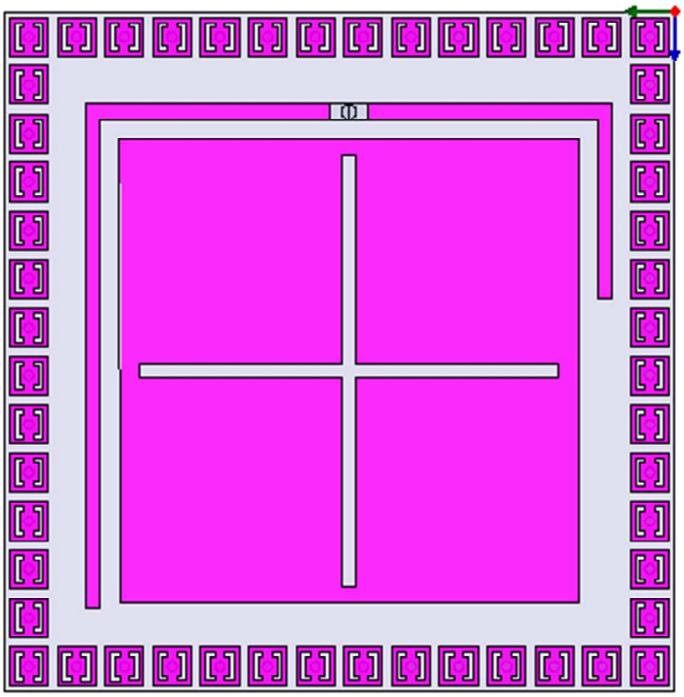

(a)

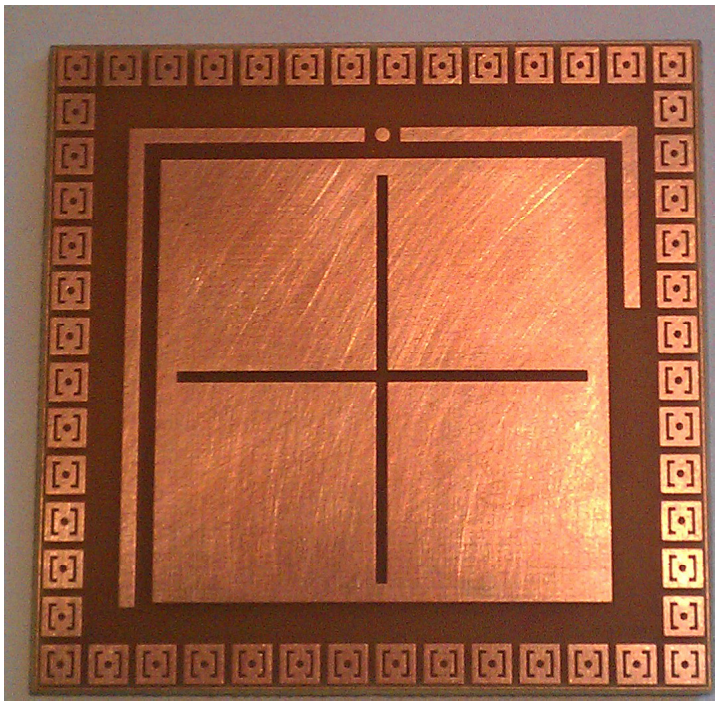

(b)

Figure 5.2: (a) Geometry and (b) fabricated prototype of the proposed Antenna-II

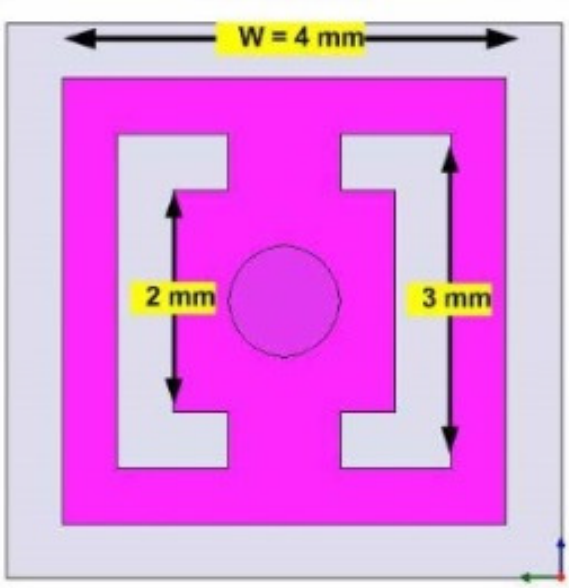

Figure 5.3: EBG structure used in Antenna-II

5.3. Results and discussion

The proposed antenna is designed for Impinj Monza Gen2 tag chip which has an input impedance of 33-j112Ω at 915 MHz [Monza4 Tag]. All the simulations are performed using the Ansys high frequency structure simulator (HFSS) [HFSS ver. 14.0] that uses Finite Element Method (FEM) as the numerical technique to solve the EM problems.The optimized values of the shape parameters of the proposed antenna are shown in Table 5.1.

Table 5.1 Geometrical dimensions of the proposed antenna

Parameter	Value (mm)	Parameter	Value (mm)
G	70	Ly5	1.35
t	1.5	Lx1	25.5
Ly1	52	Lx2	25.5
Ly2	20	Lx3	48
Ly3	21.5	Lx4	2
Ly4	21.5	g	1.5

5.3.1. Parametric Study

The real and imaginary parts of the input impedance of the receiving Antenna-I by tuning the parameter *Ly*1 by keeping other parameters at their optimized value are shown in Figures 5.4(a) and 5.4(b), respectively. It is observed that the real part of the input impedance of the receiving Antenna-I, is equal to 33.2 Ω and the imaginary part is j111.2 Ω at 915 MHz frequency which is close to the complex conjugate of the chip impedance (33-j112) Ω. This shows that how the receiving antenna parameters of the tag are carefully designed to provide a good conjugate match with the chip impedance at 915 MHz frequency. The proper impedance value of the antenna is required to minimize the reflection losses between antenna and chip, and hence, improve the power transmission and maximize the read range.

To understand the maximum power transfer phenomena of the RFID tag, power reflection and transmission coefficients are calculated as described by Nikitin *et al.* [Nikitin *et al.* (2005)]. The Variation of simulated power reflection coefficient and power transmission coefficient of receiving Antenna-I by varying the parameter *Ly*1 is presented in Figures 5.5 and 5.6, respectively. It is observed that at 915 MHz frequency, the power reflection coefficient is minimum, and the value of power transmission coefficient is maximum. This indicates that the maximum power is transferred from tag antenna to chip.

Figures 5.7(a) and 5.7(b) show the real and imaginary part of the input impedance of the receiving Antenna-I whereas, Figure 5.7(c) shows the imaginary part of the input impedance of the backscattering Antenna-I by tuning the parameter 'g' and keeping other parameters at their optimized values. It is observed that, at a frequency of 915 MHz, the real and imaginary part of the input impedance of receiving Antenna I and imaginary part of backscattering Antenna I are easily tuneable to achieve the complex conjugate of the chip impedance.

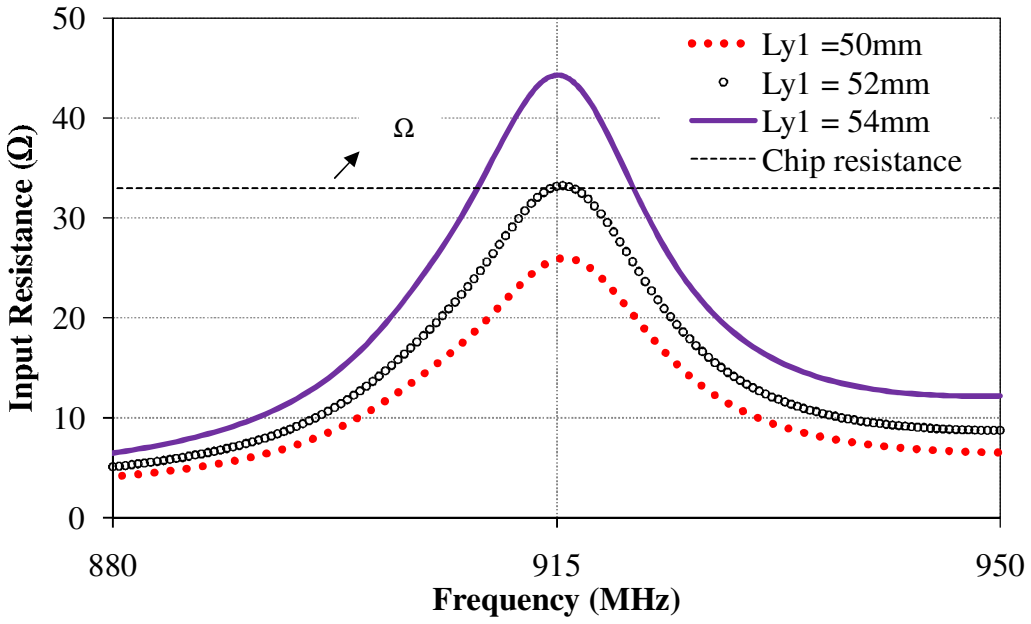

(a)

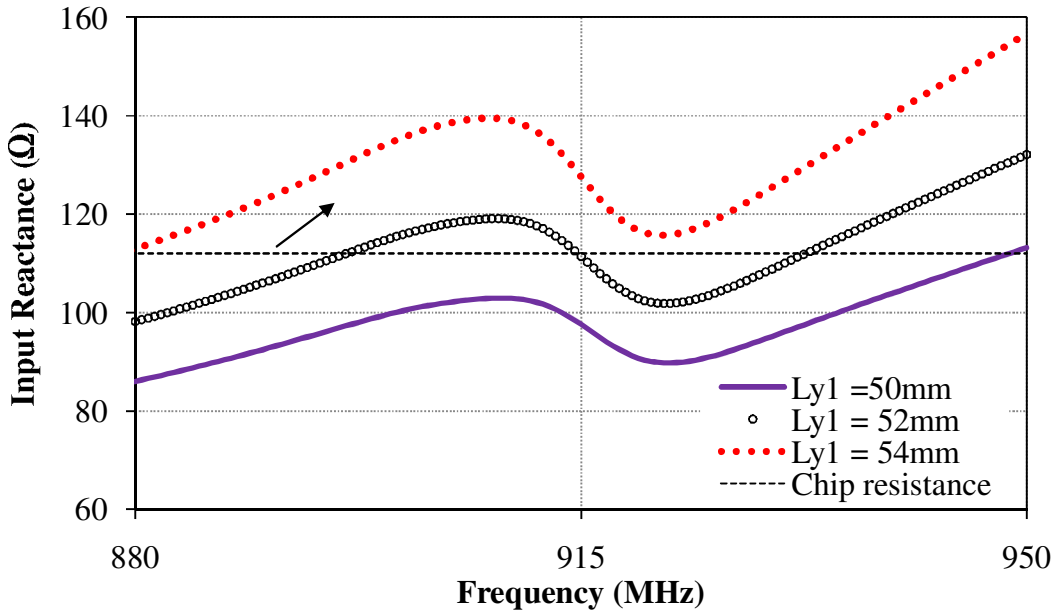

(b)

Figure 5.4: Simulated input impedance of receiving Antenna-I by tuning the L*y*1 (a) input resistance and (b) input reactance.

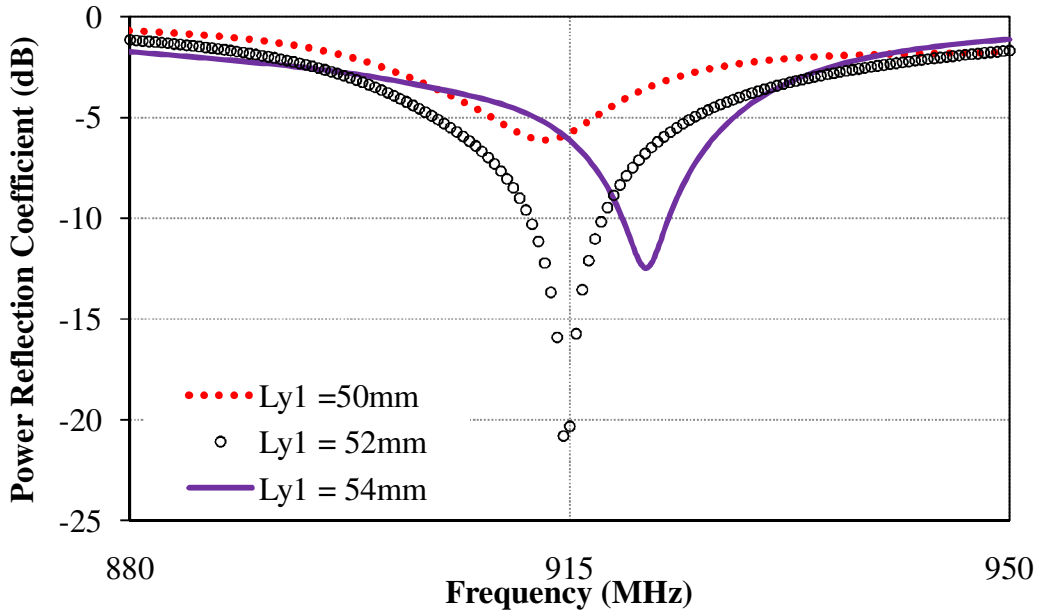

Figure 5.5: Simulated Power Reflection Coefficient of receiving Antenna-I by tuning the L*y*1.

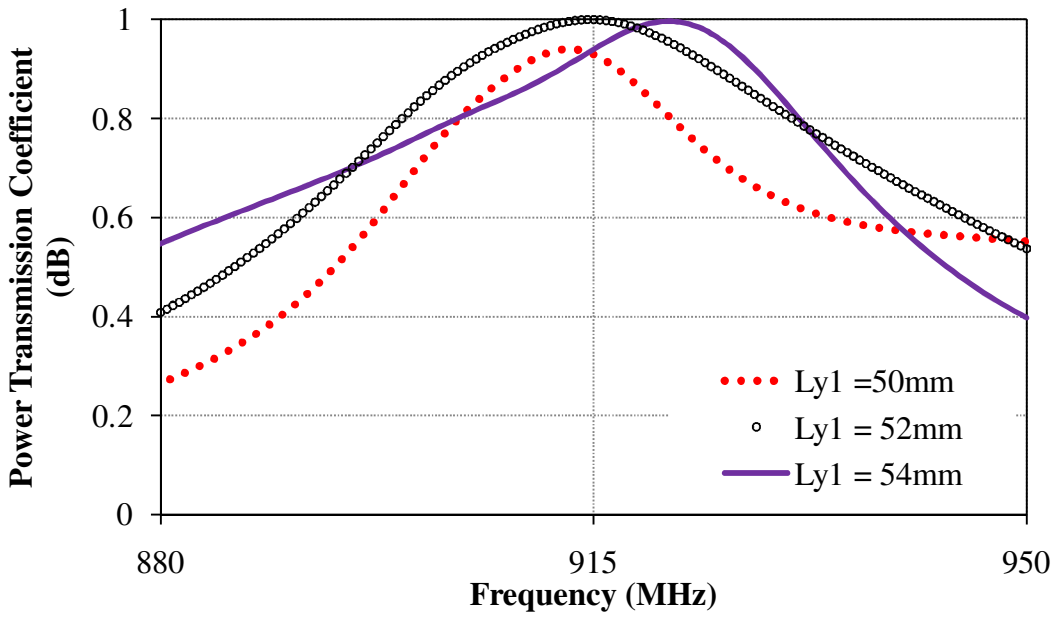

Figure 5.6: Simulated Power Transmission Coefficient receiving Antenna-I by tuning the L*y*1.

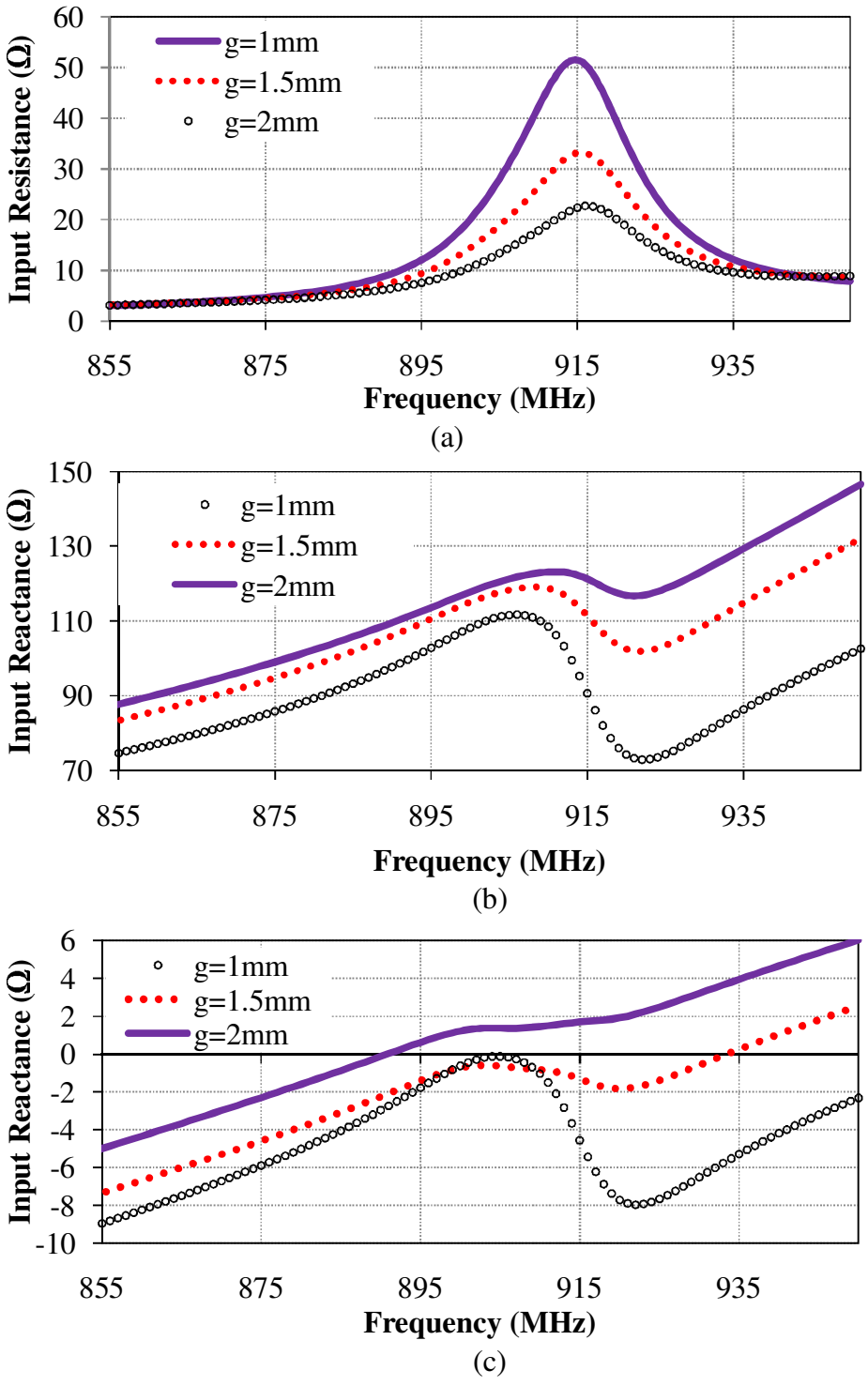

Figure 5.7: Simulated input impedance of receiving and backscattering Antenna-I by tuning 'g' (a) input resistance of receiving antenna and (b) input reactance of receiving antenna and (c) input reactance of backscattering antenna.

Figures 5.8(a) and 5.8(b) show the real and imaginary part of the input

impedance of the receiving Antenna-I whereas, Figure 5.8(c) shows the imaginary part of the input impedance of the backscattering antenna by tuning the width of the cross-shaped slot (Ly5) by keeping optimized values for other parameters. It is observed that the resonance point corresponding to the complex conjugate of the chip impedance decreases with the increase of the width Ly5 in the case of receiving Antenna-I whereas in the case of backscatter Antenna-I reactance of the antenna approaches to zero ohm.

Figure 5.9 shows the variation of imaginary part of the input impedance with frequency for the backscattering Antenna-I by varying the vertical length (Ly2), while the receiving antenna is matched terminated. The imaginary part of backscattering antenna should be close to zero for maximum differential RCS and the value of reactance close to zero (-1.3 Ω) is obtained.

Figures 5.10(a) and 5.10(b) show the real and imaginary part of the input impedance of the receiving Antenna-I whereas, Figure 5.10(c) shows the imaginary part of the input impedance of the backscattering antenna by tuning the width of the microstrip line (t) by keeping optimized values for other parameters. It is observed that at 915 MHz frequency, the imaginary part of the input impedance of both the antennas is tuneable towards its reactance value while the real part of the input impedance of receiving antenna is unchanged.

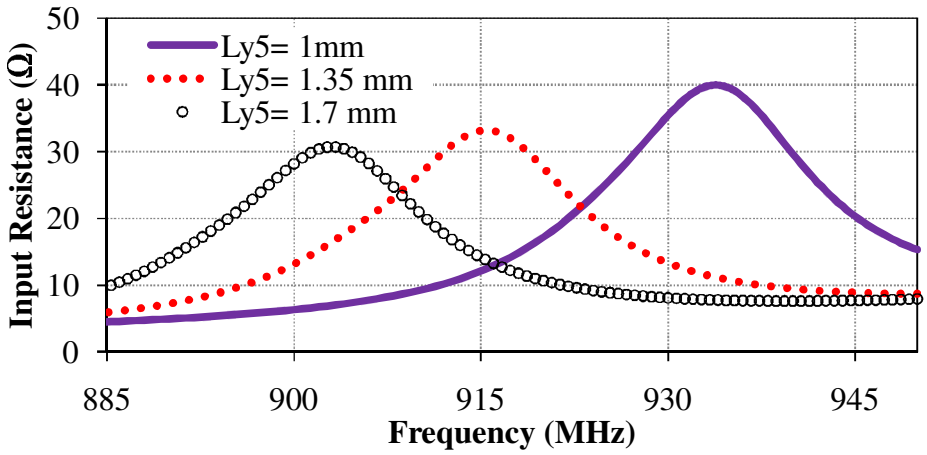

(a)

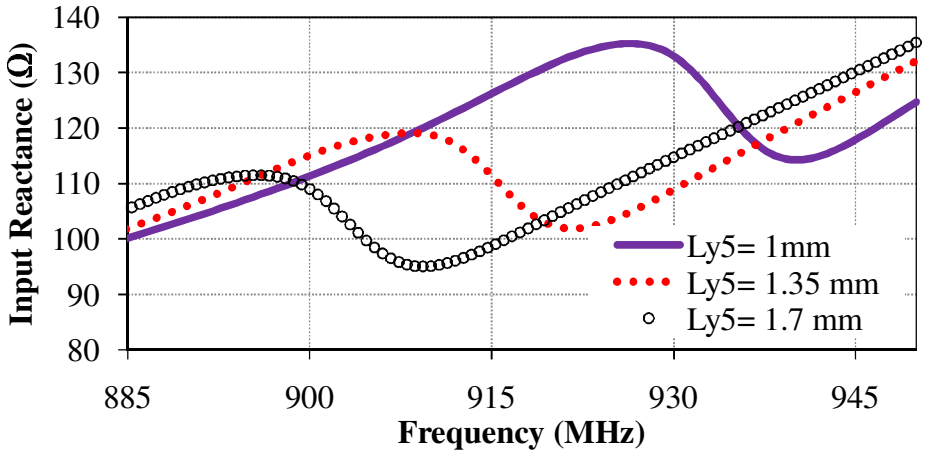

(b)

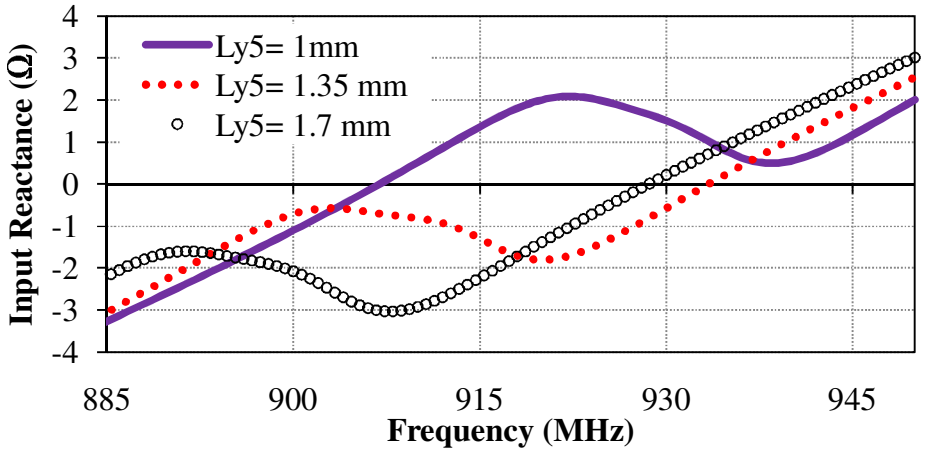

(c)

Figure 5.8: Simulated input impedance of receiving and backscattering Antenna-I by tuning the Ly5 (a) input resistance of receiving antenna and (b) input reactance of receiving antenna and (c) input reactance of backscattering antenna.

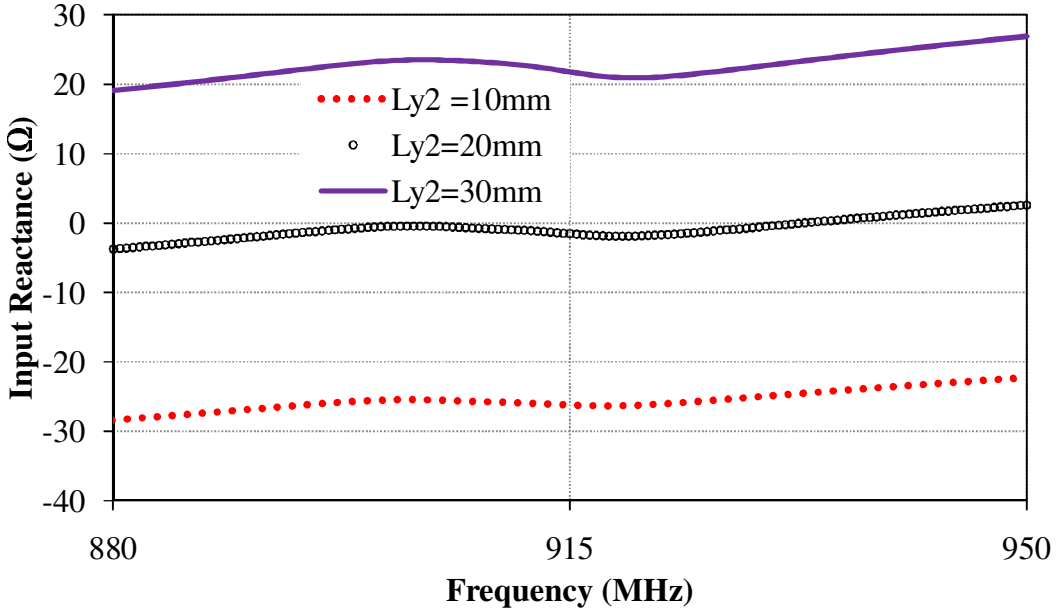

Figure 5.9: Simulated input reactance of backscattering Antenna-I by tuning the L*y*2.

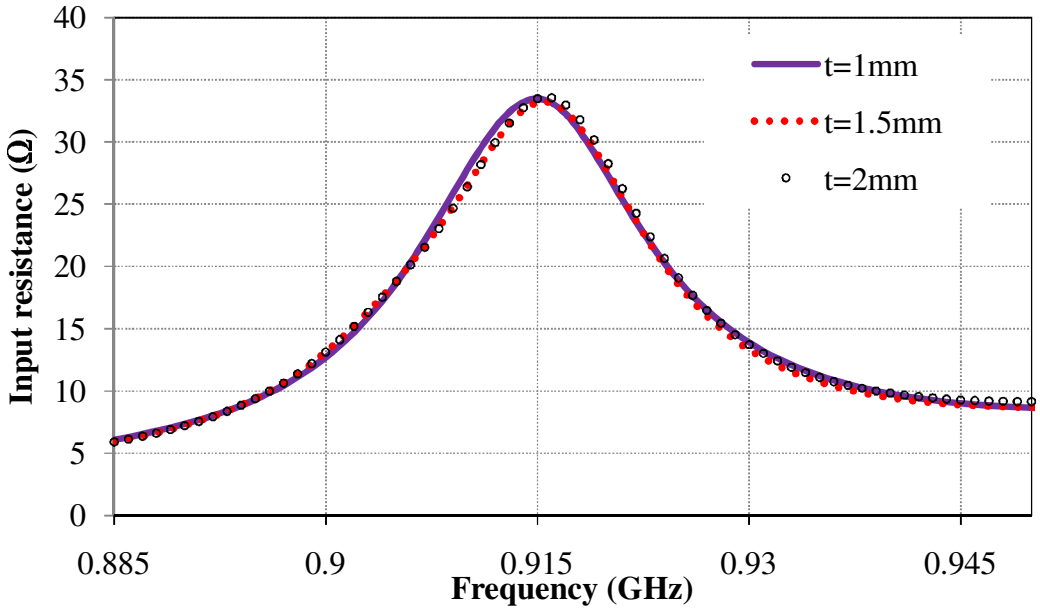

(a)

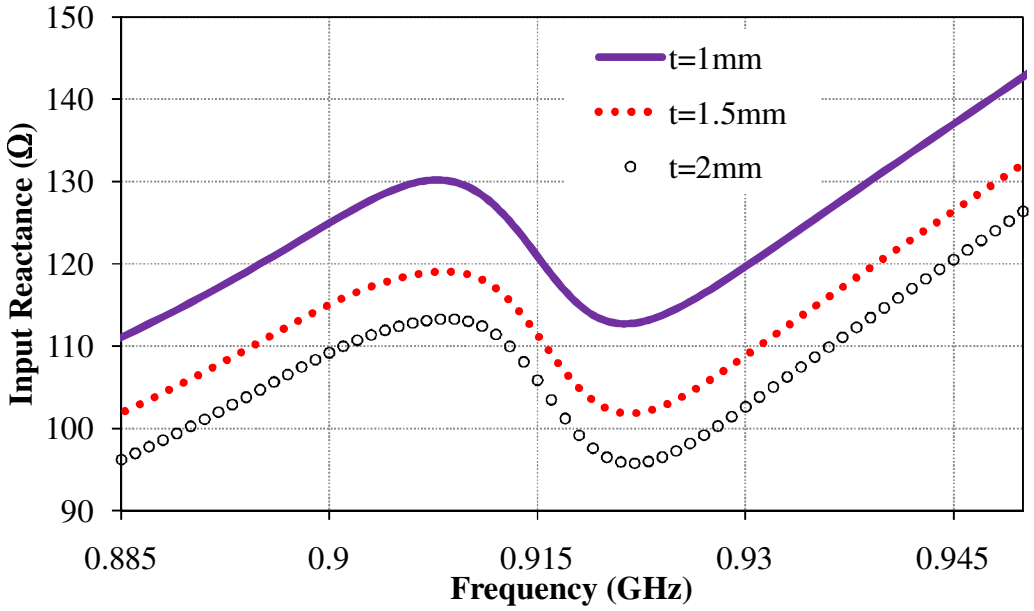

(b)

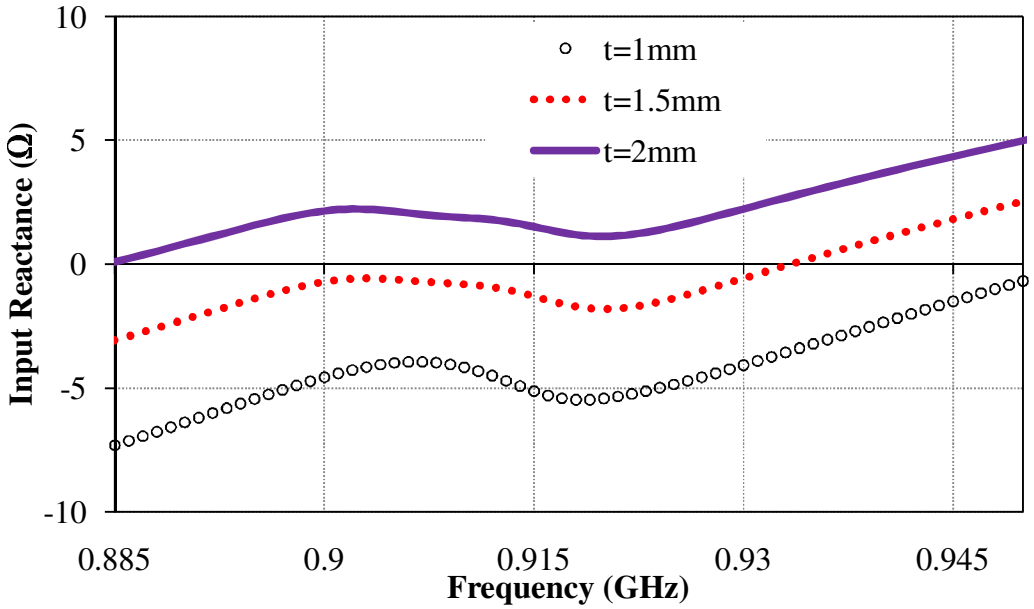

(c)

Figure 5.10: Simulated input impedance of receiving and backscattering Antenna-I by tuning the t (a) input resistance of receiving antenna and (b) input reactance of receiving antenna and (c) input reactance of backscattering antenna.

5.3.2. Simulation and Measurement Results

To measure the characteristics of the proposed RFID tag antennas, we have fabricated the differential probe as mentioned in [Qing *et al.* (2009)a, Koskinen *et al.* (2009), Palmer and Rooyen (2006)] which is shown in Figure 5.11(a). Figure 5.11(b) shows the measurement setup. With the help of differential probe connected to the terminals of the antenna, *S*-parameters for two ports of the differential probe are measured and using the values of the *S*-parameters, the differential input impedance is calculated. Further, with the help of differential input impedance, power reflection coefficient is calculated [Nikitin *et al.* (2005)]. Figures 5.12 and 5.13 show the simulated and measured results of input impedance and power reflection coefficient for receiving Antenna-I and Antenna-II. The measured complex input impedances for the receiving antennas of Antenna-I and Antenna-II are obtained as 25.4 + j115.18 Ω and 24 + 114.35 Ω, respectively, which are close to the complex conjugate of the chip impedance i.e. (33 + j112 Ω). The simulated and measured input reactance of backscatter of Antenna-I and Antenna-II are shown in Figure 5.14. The measured reactance values of the backscattering antenna for Antenna-I and Antenna-II are observed as -0.49 Ω and -1.121 Ω, respectively which are close to zero. The simulated and measured results are in good agreement as seen from the plots.

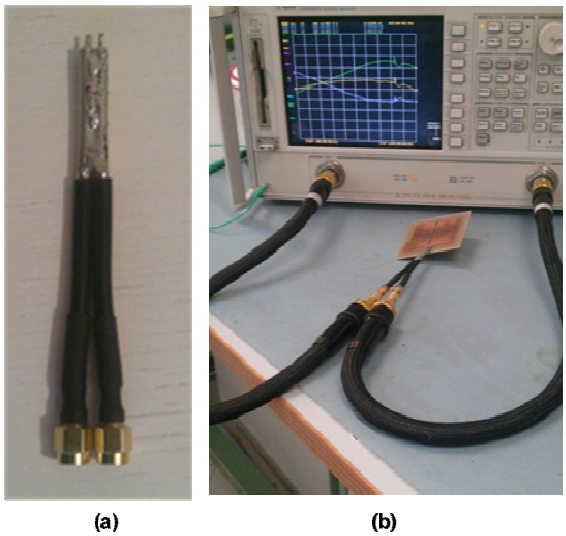

Figure 5.11: (a) Differential probe and (b) measurement setup

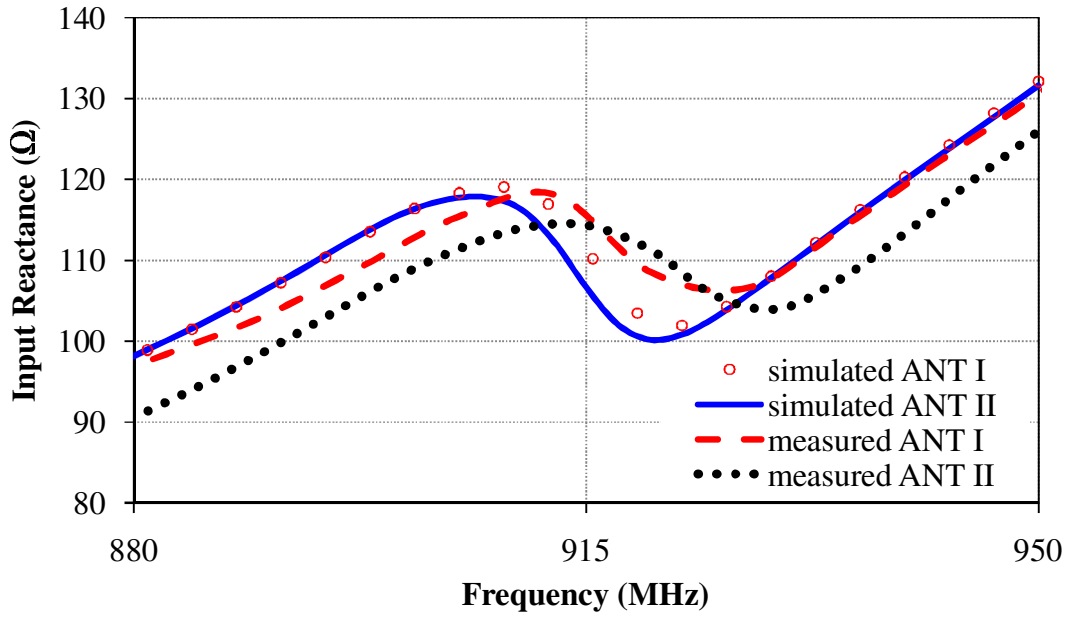

(a)

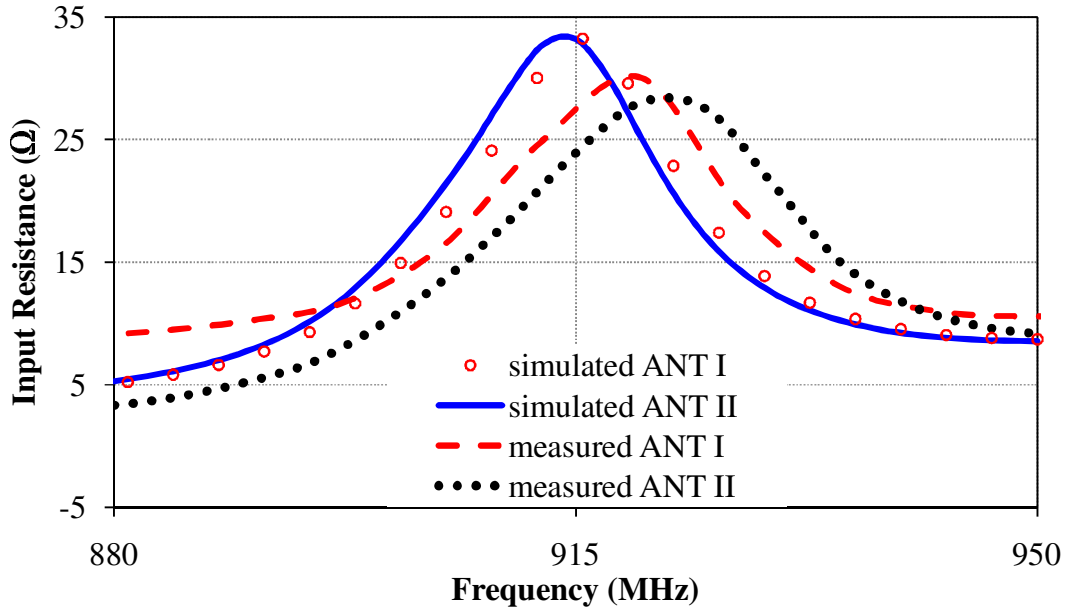

(b)

Figure 5.12: Simulated and measured (a) input reactance of Antenna-I and Antenna-II, (b) input resistance of Antenna-I and Antenna-II

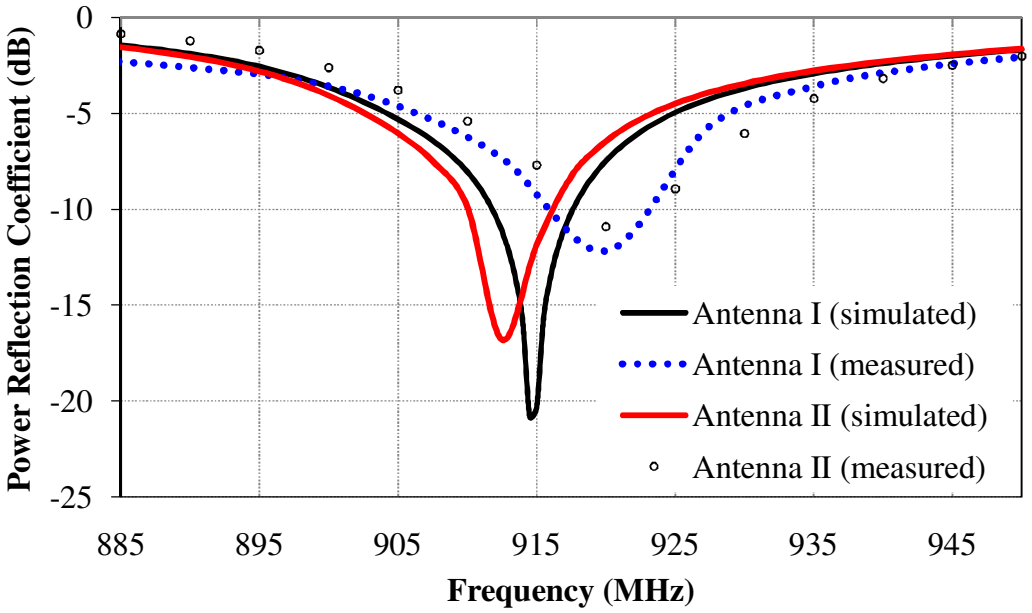

Figure 5.13: Simulated and measured power reflection coefficient of proposed Antenna-I and Antenna-II

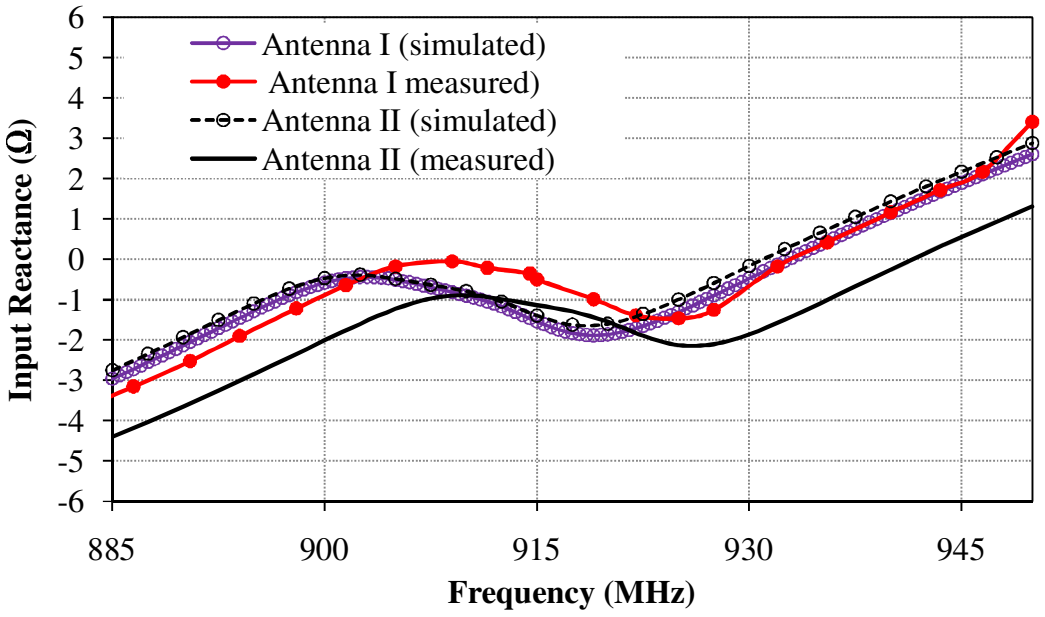

Figure 5.14: Simulated and measured input reactance of backscattering Antenna-I and Antenna-II

Figure 5.15 shows the isolation between receiving and backscattering antenna for both Antenna-I and Antenna-II. It is observed that isolations in both the cases are almost identical, and value of isolation at 915 MHz is better than -20 dB.

The simulated realized gain of Antenna-I and Antenna-II are shown in Figure 5.16. It is observed that the maximum realized gain of Antenna-I and Antenna-II at 915 MHz in free space is -14.1 dBi and -12 dBi. It is clear that using EBG structures, insignificant effect is observed on complex conjugate of the chip impedance (i.e., from 33+j111 to 33+j106) at 915 MHz frequency as shown in Figure 5.13 and results in considerable enhancement of gain and read range from -14.2 dBi to -12 dBi and 4.3 m to 5.5 m, respectively.

RCS of proposed dual Antenna-I is compared with the conventional single antenna structure in Figures 5.17 and 5.18. It is observed that differential RCS ($\Delta\sigma$) in two states (open and short) of proposed Antenna-I is increased, which results in enhancement of read range as shown in Figure 5.19. Since, the read range is directly proportional to the differential RCS, therefore, for the increase in $\Delta\sigma$ from 15 dBsm to 93 dBsm, the read range increases from 3.6 m to 4.3 m.

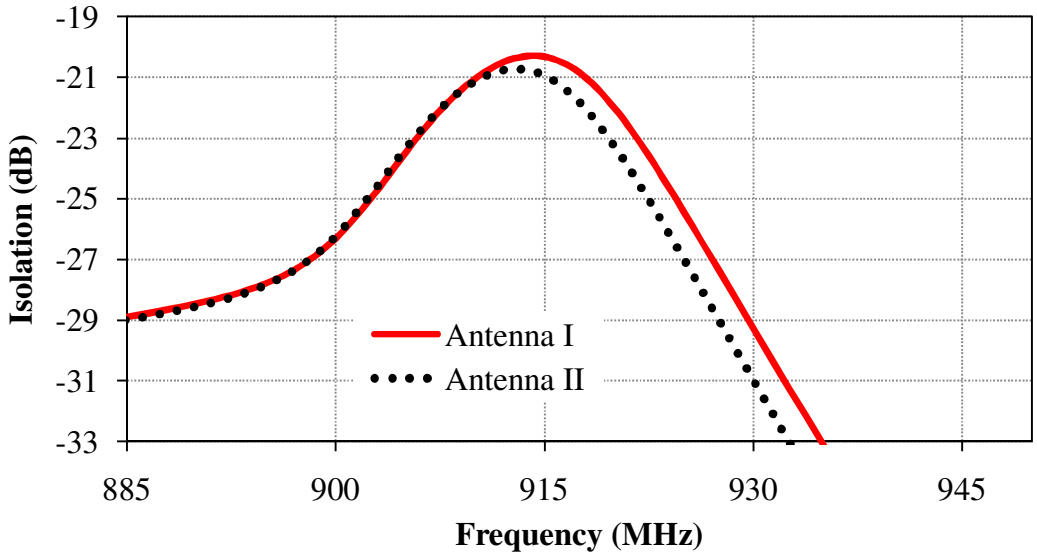

Figure 5.15: Isolation between receiving and backscattering antenna for Antenna-I and Antenna-II

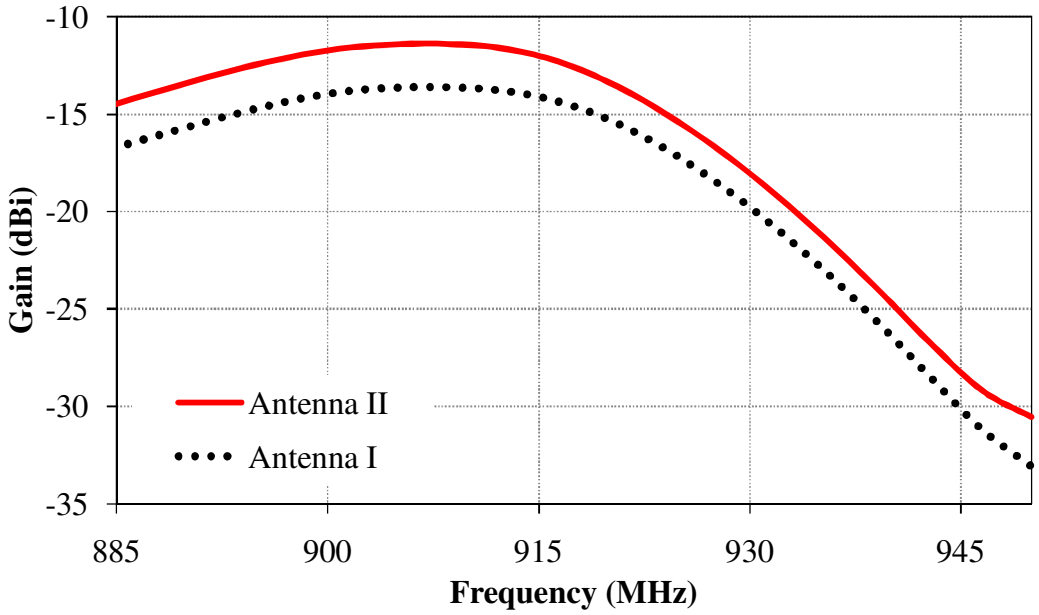

Figure 5.16: Realized gain of Antenna-I and Antenna-II

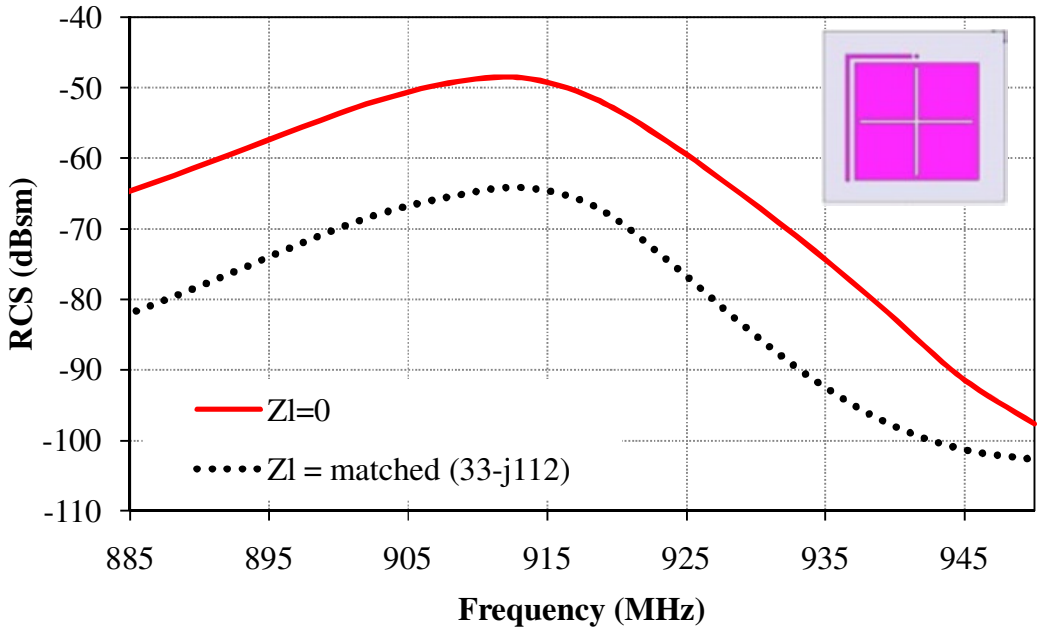

Figure 5.17: RCS of conventional single antenna in two states (open and short circuit)

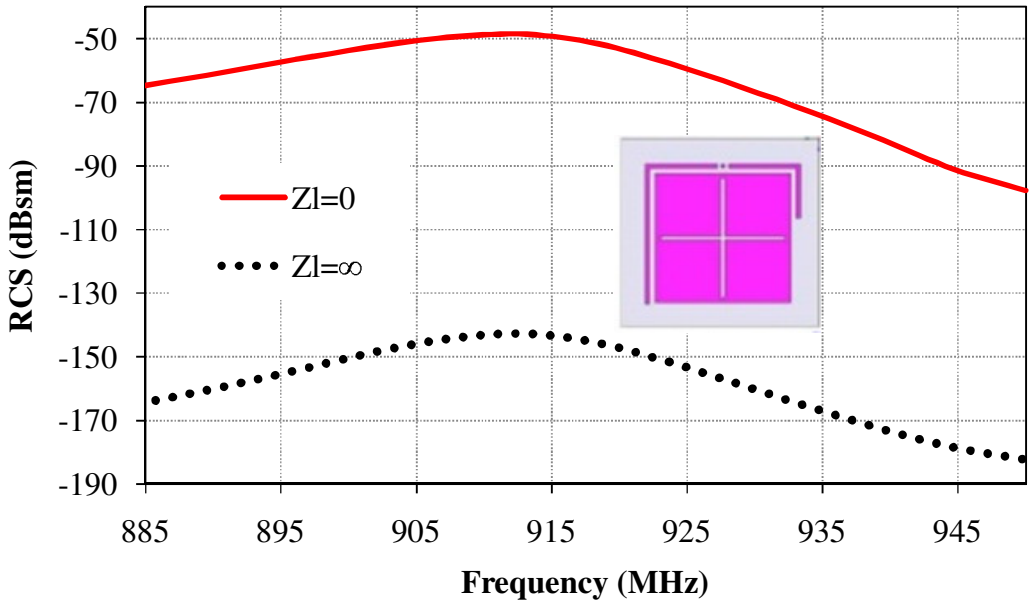

Figure 5.18: RCS of proposed Antenna-I in two states (open and short circuit)

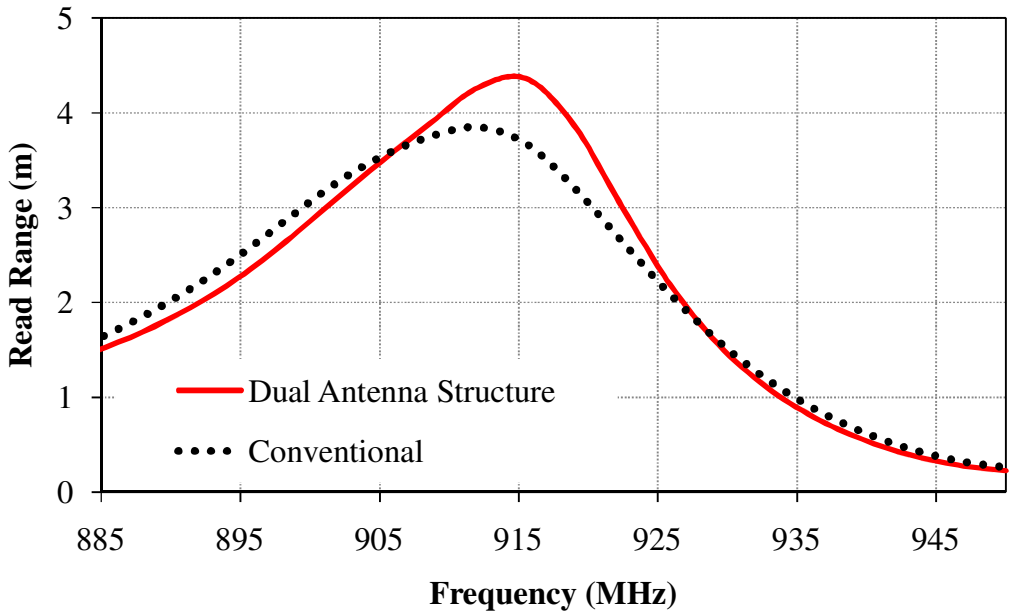

Figure 5.19: Read range comparison of conventional and proposed Antenna-I

Figure 5.20 shows the surface current distribution for Antenna-I and Antenna-II at 915 MHz. It is observed that using EBG structure around Antenna-I, the surface wave propagation is minimized and increased the surface current distribution on the antenna elements which results in improvement in the gain, read range, radiation efficiency, and radiation pattern of the antenna. The read range of Antenna-I and Antenna-II is shown in Figure 5.21. It is observed that with the use of EBG structures, the gain and read range significantly increases.

Figure 5.22 shows the simulated radiation patterns of receiving and backscattering of Antenna-I and Antenna-II at 915 MHz. All the radiation patterns are normalized with reference to maximum radiated field. It is observed that for both the Antenna-I and Antenna-II, the E_ϕ component in x-z plane and E_θ component in y-z plane dominates over the E_θ and E_ϕ, respectively. Further, with the use of EBG like structure in the Antenna-II, the radiation pattern due to the dominant components improves with a significant reduction in side lobes and more radiation in the boresight direction ($\theta = 0^0$) is observed whereas less effect is observed on the other field components.

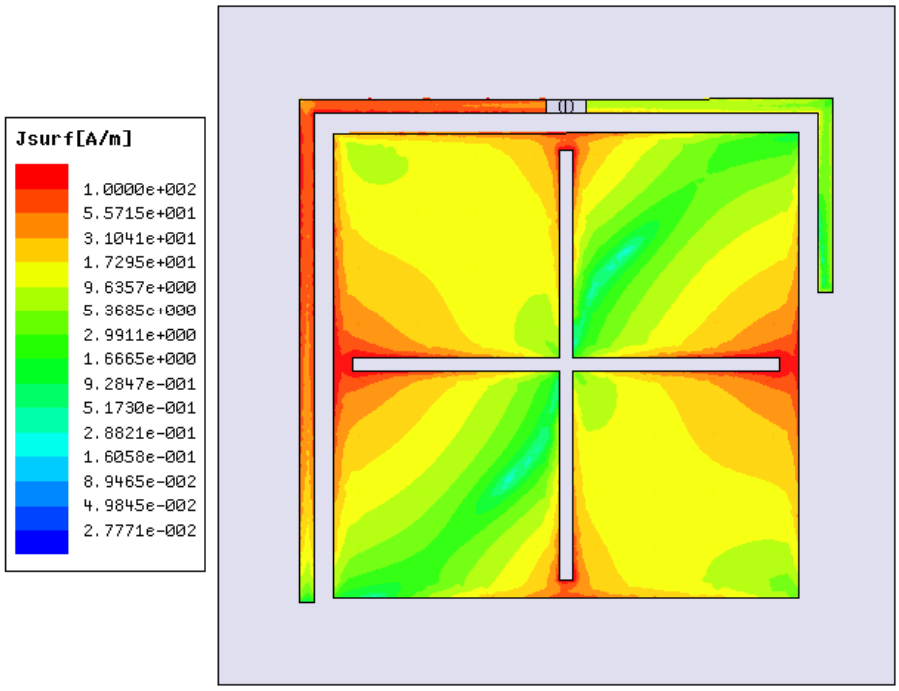

(a)

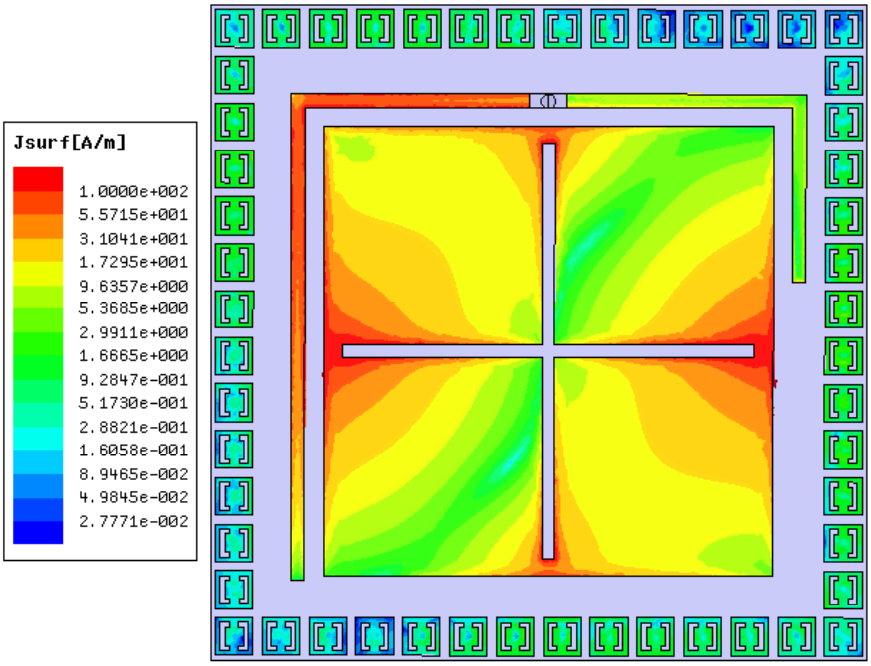

(b)

Figure 5.20: Surface current distribution on 915 MHz for (a) Antenna-I and (b) Antenna-II

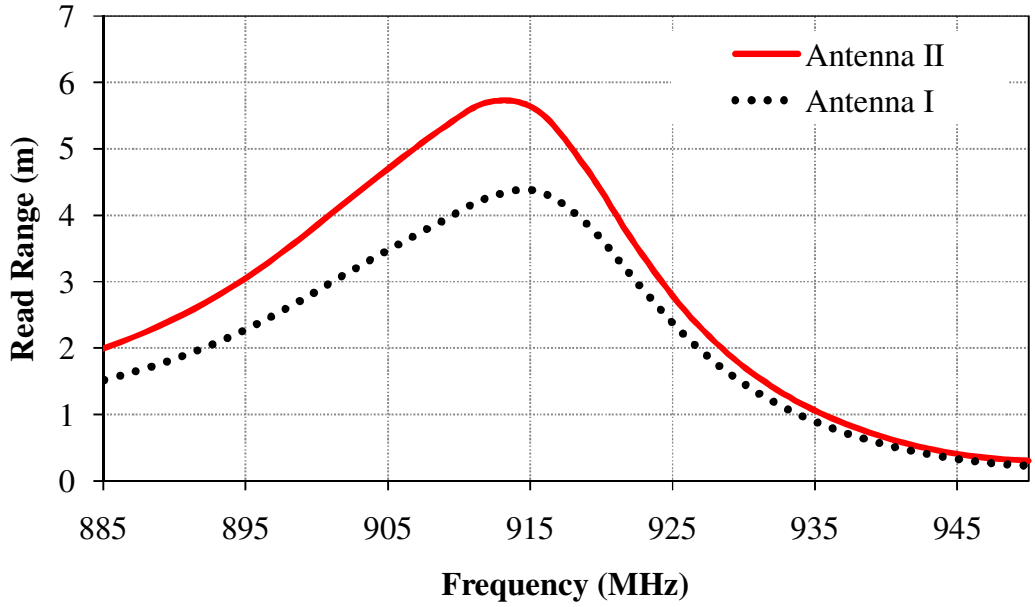

Figure 5.21: Read range of Antenna-I and Antenna-II

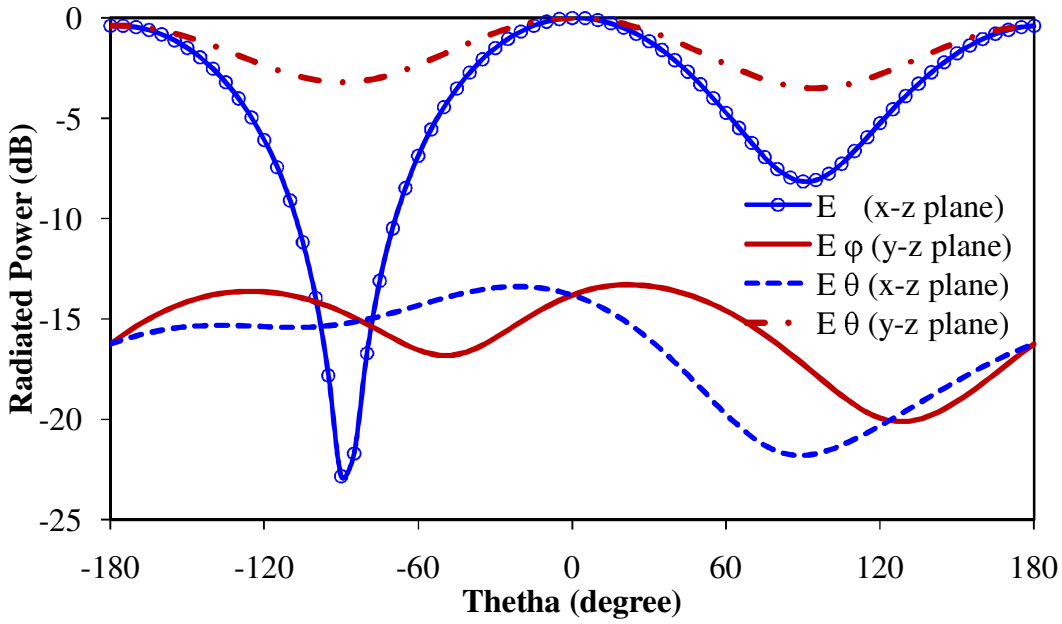

(a)

Figure 5.22(a): Simulated radiation patterns of receiving Antenna-I.

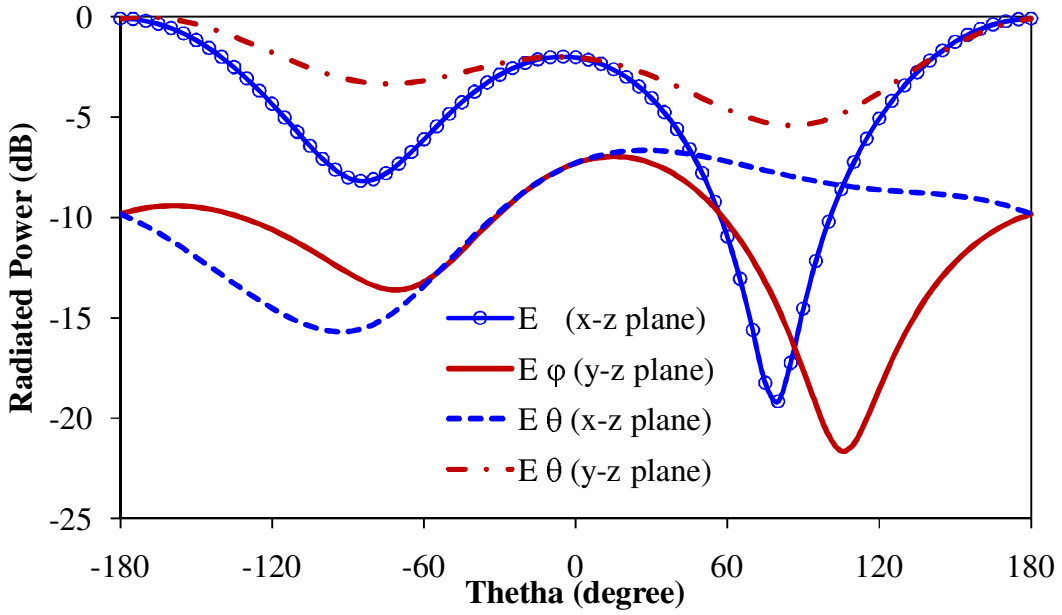

(b)

Figure 5.22 (b)**:** Simulated radiation patterns of backscattering of Antenna-I.

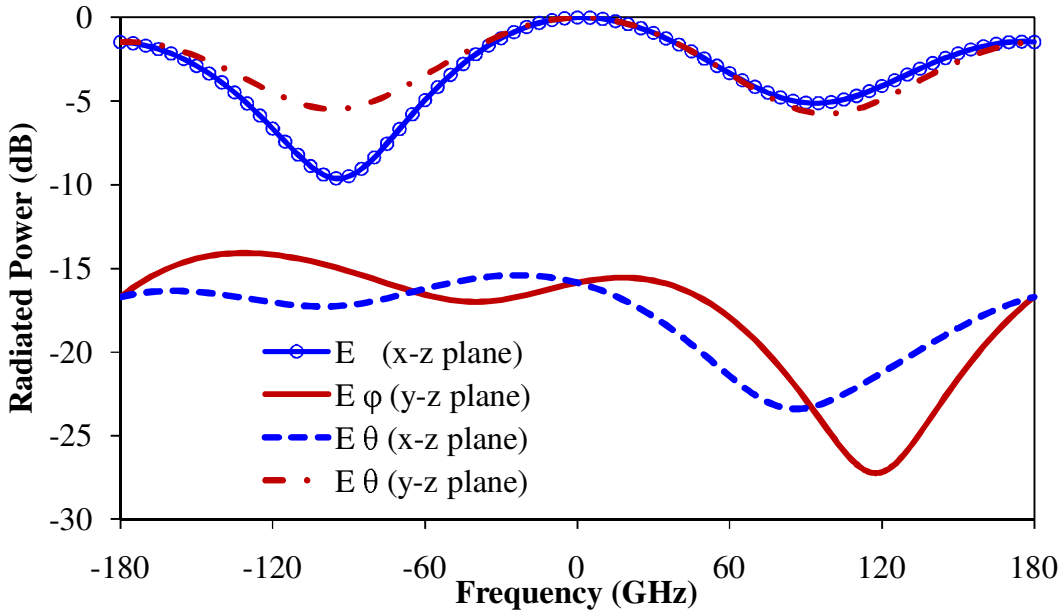

(c)

Figure 5.22 (c): Simulated radiation patterns of receiving Antenna-II.

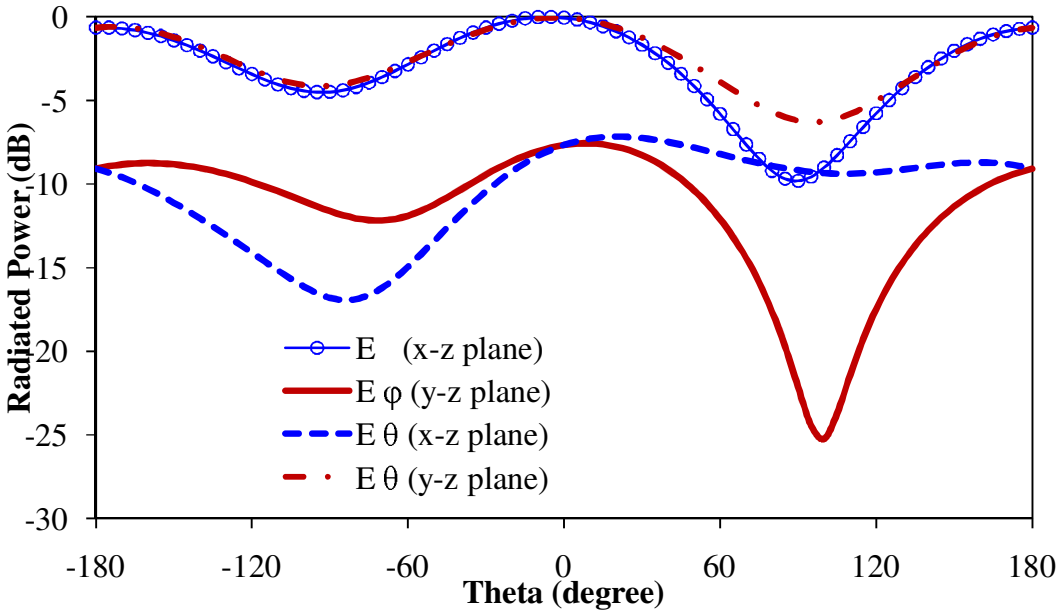

(d)

Figure 5.22 (d)**:** Simulated radiation patterns of backscattering of Antenna-II.

5.3.3. Effect of mounting material on RFID tag antenna

To see the effect of mounting of the RFID tag antenna on surfaces of different materials like metallic surface, glasses, plastic, and wood, simulation studies are carried out. For the simulation studies, the size of all the material objects is of equal size but bigger than the ground plane. The value of relative permittivity and conductivity of these materials are given in Table 5.2. Gain and read range of the proposed Antenna-I and Antenna-II along with when Antenna-II is attached on different material surfaces is summarized in Table 5.3. The results show that gain and read range of the proposed antenna increases remarkably when placed on a metallic surface, though the best performance occurs when the surface is made of glass which has maximum relative permittivity comparatively. Figure 5.23, show the variation of gain and read range of Antenna-II on different material with variation in frequency.

Table 5.2: Properties of different materials [ANSYS HFSS]

Material name	Glass	Plastic	Wood	Metal	Air
Relative permittivity (ε_r)	5.5	3.5	2.5	1	1
Conductivity (Siemens/m)	0	0	0	58000000	0

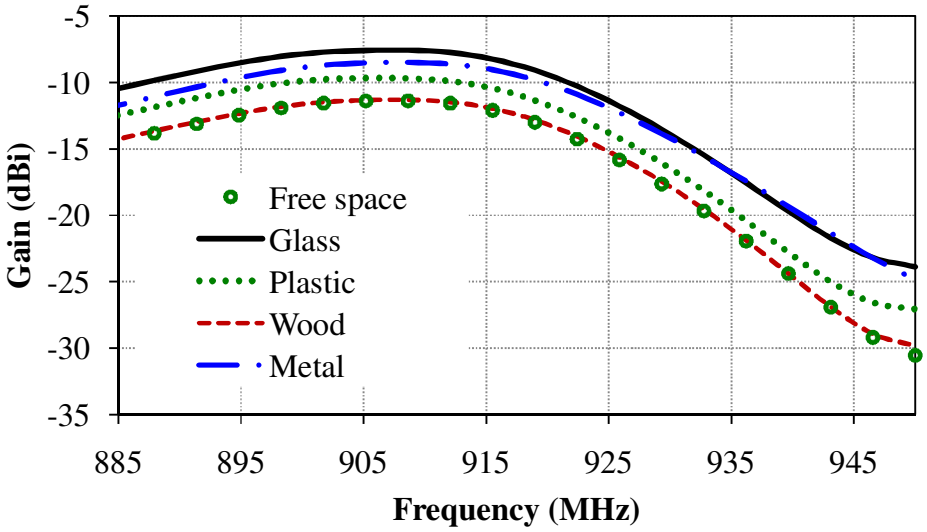

(a)

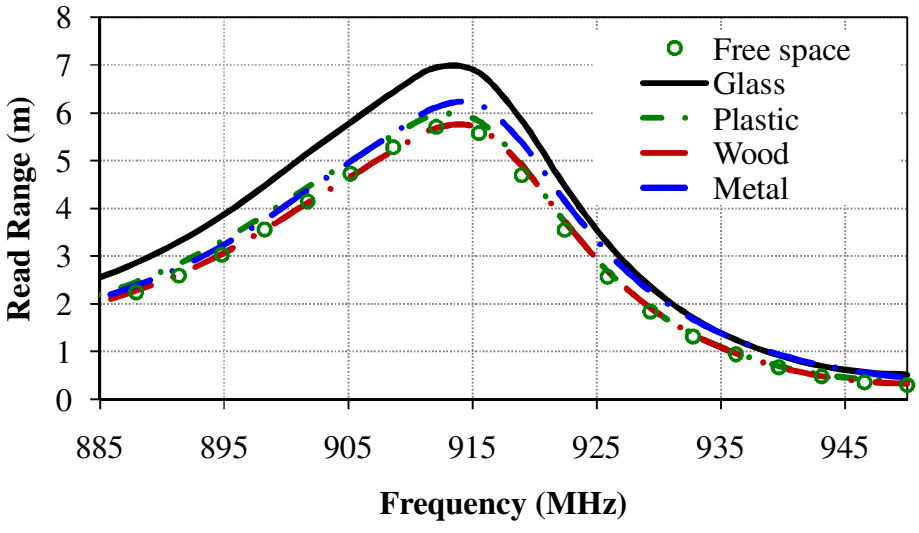

(b)

Figure 5.23: (a) Gain and (b) read range of Antenna-II on Free space, Glass, Plastic, Wood and Metal.

Table 5.3 Gain and read range of antennas in different conditions

	Ant-I	Ant-II	Ant-II on wood	Ant-II on plastic	Ant-II on metal	Ant-II on glass
Gain (dBi)	-14	-12	-11.9	-10.4	-9	-8.4
Read range(m)	4.3	5.5	5.6	5.8	6.1	6.8

5.4. Summary

A dual-structure UHF RFID tag antenna was presented in this chapter. The major objective of such design was to increase the read range, using two techniques. First, used the dual-antenna structure to increase the Δ RCS and second, use of EBG structure to increase the gain. The proposed antenna is suitable to be used when mounted on the metallic surfaces. The input impedance of receiving antenna of the antenna is 33.2+j111.2 Ω at 915 MHz. The Δ RCS and maximum read range of dual antenna are 93 dBsm and 4.3 m while the gain and read range of dual antenna with EBG- structure is -12 dBi and 5.5 m, respectively. The measured results are in good agreement with the simulated results.